Correlating the Plasmonic and Structural Evolutions during the Sulfidation of Silver Nanocubes

Caihong Fang,[†,§] Yih Hong Lee,[‡,§] Lei Shao,[†] Ruibin Jiang,[†] Jianfang Wang,[†,*] and Qing-Hua Xu[‡,*]

[†]Department of Physics, The Chinese University of Hong Kong, Shatin, Hong Kong SAR, China and [‡]Department of Chemistry, National University of Singapore, 3 Science Drive 3, Singapore 117543. [§]C. H. Fang and Y. H. Lee contributed equally to this work.

ABSTRACT Ag/Ag_2S hybrid nanostructures have recently received much attention, because of their synthetically tunable plasmonic properties and enhanced chemical stability. Sulfidation of pregrown Ag nanocrystals is a facile process for making Ag/Ag_2S nanostructures. Understanding the sulfidation process can help in finely controlling the compositional and structural parameters and in turn tailoring the plasmonic properties. Herein we report on our study of the structural and plasmonic evolutions during the sulfidation process of Ag nanocubes, which is carried out at both the ensemble and single-particle levels. Ensemble extinction measurements show that sulfidation first causes the disappearance of the high-order triakontadipolar plasmon modes, which have electric charges located on the sharp vertices and edges of Ag nanocubes, suggesting that sulfidation starts at the vertices of Ag nanocubes. As sulfidation goes on, the dipolar plasmon peak gradually red-shifts, with its intensity first decreasing and then increasing. Electron microscopy characterizations reveal that sulfidation progresses from the outer region to the center of Ag nanocubes. The cubic shape is maintained throughout the sulfidation process, with the edge length being increased gradually. Single-particle scattering measurements show that the dipolar plasmon peak red-shifts and decreases in intensity during sulfidation. An additional scattering peak appears at a shorter wavelength at the late stage of sulfidation. The difference in the sulfidation behavior between ensemble and single-particle measurements is understood with electrodynamic simulations. During ensemble measurements, the Ag core is increasingly truncated, and it becomes a nanosphere eventually. Sulfidation stops at an intermediate stage. During single-particle measurements, Ag nanocubes are completely transformed into Ag_2S, leading to the observation of the shorter-wavelength scattering peak.

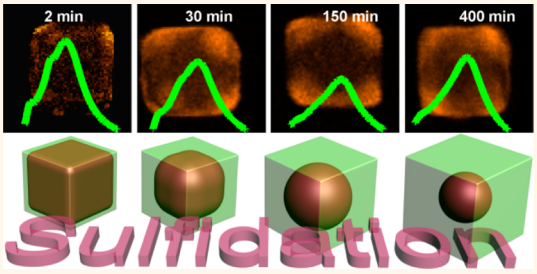

KEYWORDS: dark-field scattering · extinction · finite-difference time-domain method · microfluidics · plasmon · silver nanocubes · sulfidation

Localized surface plasmon resonances of noble metal nanocrystals have enabled a spectacular variety of phenomena and applications, which include enhanced fluorescence and Raman scattering, biological imaging and phototherapy, optical data storage, and various sensing technologies.[1,2] Arising from the collective oscillations of the electrons in the conduction band, localized surface plasmon resonances of noble metal nanocrystals are strongly dependent on the nanocrystal morphology and surrounding dielectric environment. In particular, the refractive index sensitivities of noble metal nanocrystals are well documented and have been investigated intensively.[3−5] Refractive index sensitivities exceeding 1000 nm/RIU have been reported for Ag nanoplates,[6] and figure-of-merit values exceeding 100 have been demonstrated for lithographically fabricated metal structures possessing Fano resonances.[7] In the visible region, Ag has been shown to be twice as sensitive to dielectric changes as Au when nanocrystals of both metals with similar sizes and plasmon resonances are compared.[8] Even though Ag is a superior metal for sensing, its applications are limited by the instability of the metal to structural truncation and oxidation over time.[9,10]

To address the instability of Ag nanocrystals, they have often been hybridized with semiconductors such as Ag_2S through various synthetic methods. Sulfidation of Ag nanoprisms and nanocubes has been demonstrated to improve both the structural and thermal stability of the Ag nanocrystals.[11] The addition of a semiconductor shell changes

* Address correspondence to jfwang@phy.cuhk.edu.hk; chmxqh@nus.edu.sg.

Received for review August 3, 2013 and accepted September 13, 2013.

Published online September 13, 2013
10.1021/nn404042p

the surrounding dielectric environment of the metal core, which therefore also serves as a route for the plasmon resonances to be continuously tuned across the entire visible range. Moreover, the integration of Ag nanocrystals with Ag_2S brings about novel hybrid (metal core)/(semiconductor shell) nanomaterials with improved application performances. By itself, Ag_2S is an intriguing material with many outstanding properties. Its narrow band gap (~1 eV), high absorption coefficient, good chemical stability, and efficient photoluminescence have allowed Ag_2S to be used in solar cells,[12−14] as photocatalysts,[15,16] as well as bioimaging agents.[17−21] Ag_2S has also been used in a variety of devices, including photoconductors,[22] IR detectors,[23] and superionic conductors.[24−26] Incorporation of Ag to create Ag/Ag_2S nanotubes has shown excellent photocatalytic activity for the degradation of methyl orange and reduction of aqueous Cr(VI).[27] A DNA detection limit of 1 pM has been achieved using Ag/Ag_2S hybrid nanoprisms, highlighting this hybrid nanomaterial as a promising probe for biosensing applications.[28] Enhanced antibacterial properties under UV irradiation have also been reported using Ag/Ag_2S heterodimers.[29]

In addition to improved application performances, sulfidation of Ag nanocrystals presents an attractive synthetic route for making both Ag/Ag_2S and Ag_2S nanomaterials with different morphologies. Direct sulfidation of Ag can occur without introducing significant changes to the original morphology of Ag nanocrystals, as shown in the cases of nanoprisms and nanocubes.[11] Through this synthetic route, the structural diversities of Ag/Ag_2S as well as Ag_2S nanocrystals have been enriched. While being an appealing synthetic route, little has been known about the process of direct Ag sulfidation, except that the reaction is initiated from the sharp tips of Ag nanocrystals in prisms and cubes.[11] Although this work also shows that sulfidation progresses toward the center of the Ag nanocrystals and is accompanied by a general red shift of the plasmon resonances, there is a lack of correlation between the exact structural changes occurring over the course of sulfidation with the changes in the plasmon resonances of the Ag nanocrystals. Achieving a clear understanding of the structural and plasmonic evolutions during the sulfidation process is important, as this will enable fine-tuning of the structural composition as well as the plasmonic properties of Ag/Ag_2S hybrid nanomaterials.

Herein, we make use of the strong dependence of localized surface plasmon resonances on the morphology and surrounding environment of metal nanocrystals to investigate the sulfidation process of Ag nanocubes. Ag nanocubes exhibit multiple plasmon resonances, providing a wealth of information that can be correlated to structural changes during sulfidation. We start with finite-difference time-domain (FDTD) simulations to elucidate the nature of every plasmon

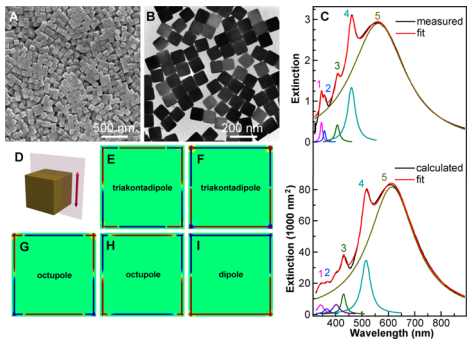

Figure 1. Ag nanocubes and their plasmon resonance modes. (A) SEM image of the Ag nanocube sample. (B) TEM image of the nanocube sample. (C) Measured (top) and calculated (bottom) extinction spectra of the Ag nanocubes. Each extinction spectrum is fitted with Lorentzian peaks. All of the peaks are individually plotted, together with their sum. The coefficients of determination for the fitting are 0.9992 and 0.9988 for the measured and calculated spectra, respectively. (D) Schematic showing the cross section through the center of the nanocube. The double-arrowed line indicates the excitation polarization direction. (E−I) Charge distribution contours (red: positive; blue: negative) on the cross section as shown in D for the five plasmon resonance peaks labeled on the extinction spectra as 1 to 5, respectively. The nature of each plasmon resonance mode is indicated on each charge distribution contour.

resonance mode arising from Ag nanocubes possessing sharp vertices and edges. Sulfidation of Ag nanocubes is monitored by tracking the spectral evolution of the extinction spectra of Ag nanocubes in solutions as well as the changes in the scattering spectra of single Ag nanocubes. Distinct changes are observed for every plasmon mode over the course of sulfidation. Intermediates formed at various points during the sulfidation process are isolated for subsequent morphological characterizations. FDTD is then used to emulate the dynamic structural changes in Ag nanocubes to account for the spectral changes during sulfidation. From the simulated data, the sulfidation of Ag nanocubes is found to occur through different pathways under the ensemble and single-particle conditions. Our presented concept and experimental data clearly indicate that localized surface plasmon resonances can be employed to unravel the chemical reaction process involving plasmonic nanocrystals and that FDTD is a valuable tool in modeling the dynamic structural changes occurring during the chemical reactions.

RESULTS AND DISCUSSION

Ag nanocubes were prepared using the polyol reduction method, where the metal salt is reduced by pentanediol in the presence of poly(vinylpyrrolidone) (PVP).[30] After centrifugation to remove pentanediol and excess PVP, the Ag nanocubes were characterized using both scanning and transmission electron microscopies (SEM and TEM, Figure 1A and B). The number yield of the nanocubes is very high, reaching up to

98%. In addition, the Ag nancubes are highly monodisperse and uniform in shape, with the average edge length measured to be 93 ± 3 nm from the TEM images. They also possess sharp vertices and edges.

The extinction spectrum of the ensemble Ag nanocube sample was measured by dispersing the nanocubes in water (Figure 1C, top). Five plasmon resonance peaks are observed. Their peak wavelengths are found from curve fitting to be 346, 358, 407, 460, and 562 nm and labeled as peaks 1 to 5, respectively. The number of observable peaks on the ensemble spectrum and their spectral positions are closely dependent on the nanocube morphology, in particular, the sharpness of the corners and vertices and the nanocube size.[31] Although five plasmon resonance peaks have also been observed previously for ensemble Ag nanocube samples,[30] the nature of the corresponding plasmon resonance modes has remained unidentified. We therefore carried out FDTD simulations to unravel the nature of the five plasmon modes. For the simulations, the Ag nanocube was set to have sharp vertices and edges, with an edge length of 93 nm. The excitation direction was along the edge of the nanocube. The refractive index of the surrounding medium was 1.33, corresponding to the index of water. Overall, the simulated extinction spectrum is in good agreement with the measured extinction spectrum (Figure 1C, bottom). There are six peaks on the simulated spectrum. Their peak wavelengths are found from curve fitting to be 343, 366, 402, 430, 515, and 613 nm, respectively. During our FDTD simulations, the dielectric function of silver was automatically generated by the software through fitting the input experimental data points. The peak at 402 nm is caused by the slight deviation of the fitted Ag dielectric function from the experimental data in the spectral region of 370 to 420 nm. It is therefore not considered in our study. The other five peaks can therefore be assigned on the basis of their peak wavelengths and intensities to the five plasmon resonance modes observed on the measured spectrum. We note that there is a wavelength difference of ~50 nm for the dipolar, smallest-energy peak between the measurements and FDTD simulations. This has been common in the numerical simulations of the extinction spectrum of Ag nanocrystals with sharp vertices and edges.[30,32] To identify the nature of the plasmon resonance modes, the charge distribution contours of the five peaks were calculated (Figure 1D–I). According to the charge distribution contours, peaks 1 to 5 can be ascribed to triakontadipolar, triakontadipolar, octupolar, octupolar, and dipolar plasmon modes, respectively. Because the charge distribution contours were calculated on the cross section passing through the center of the Ag nanocube (Figure 1D), the amounts of charges at the vertices and sides of the contours represent approximately those at the edges and surfaces that are perpendicular to the cross section on the Ag nanocube, respectively. We can therefore see that the charges of peaks 1 and 4 are mainly distributed on the surfaces of the Ag nanocube (Figure 1E and H), while those of peaks 2 and 3 are distributed on both the surfaces and edges (Figure 1F and G). The charge distribution indicates the importance of the sharp edges in the appearance of peaks 2 and 3. Slight truncation of the nanocube edges can lead to the disappearance of peaks 2 and 3, which is confirmed by our sulfidation experiments, as described below. Therefore, understanding the underlying nature of each plasmon resonance mode of metal nanocrystals can assist in correlating the spectral evolution with the structural variation of metal nanocrystals that are subjected to chemical reactions.

Sulfidation of the Ag nanocubes was realized in our study by employing an aqueous Na_2S solution as the sulfur source to react with the Ag nanocubes at room temperature. We first examined the sulfidation process of the ensemble Ag nanocube sample. Typically, an aqueous Na_2S solution was added dropwise to a washed ethanolic dispersion of the Ag nanocubes. The counting of the reaction time was started as soon as the addition of the Na_2S solution was completed. In the ensemble reaction, the particle concentration of the Ag nanocubes was estimated to be ~0.15 nM according to the supplied amount of silver and the measured average nanocube size. Different concentrations of Na_2S were used. Sulfidation of the Ag nanocubes can be described with the equation[28]

$$4Ag + O_2 + 2H_2O + 2Na_2S = 2Ag_2S + 4NaOH \quad (1)$$

The standard change of reaction in Gibbs free energy, $\Delta_r G°$, for this reaction is −491.8 kJ. Therefore, sulfidation of the Ag nanocubes will proceed spontaneously as soon as Na_2S is added in the solution. During the reaction, the pH of the solution was found to stay nearly unchanged at a basic value. This implies that NaOH is generated through the oxidation with O_2. Otherwise, the consumption of Na_2S would cause a reduction in the solution pH because Na_2S solutions are basic.

Over the course of sulfidation, the extinction spectra of the reaction solution were recorded as a function of the reaction time. Figure 2A shows the time-dependent extinction spectra acquired for the sulfidation reaction with 1 mM Na_2S. Distinct changes are observable on the extinction spectra. To reveal more clearly the spectral changes during the sulfidation process, we plotted the positions of the five peaks in Figure 2B and the extinction intensity of peak 5 in Figure 2C as functions of the reaction time. The spectral evolutions can be divided roughly into two stages. The first stage is from the start to ~10 min. At this stage, the spectral positions of the five peaks vary dramatically. Peak 2 disappears within ~2 min. Peaks 1, 4, and 5 exhibit

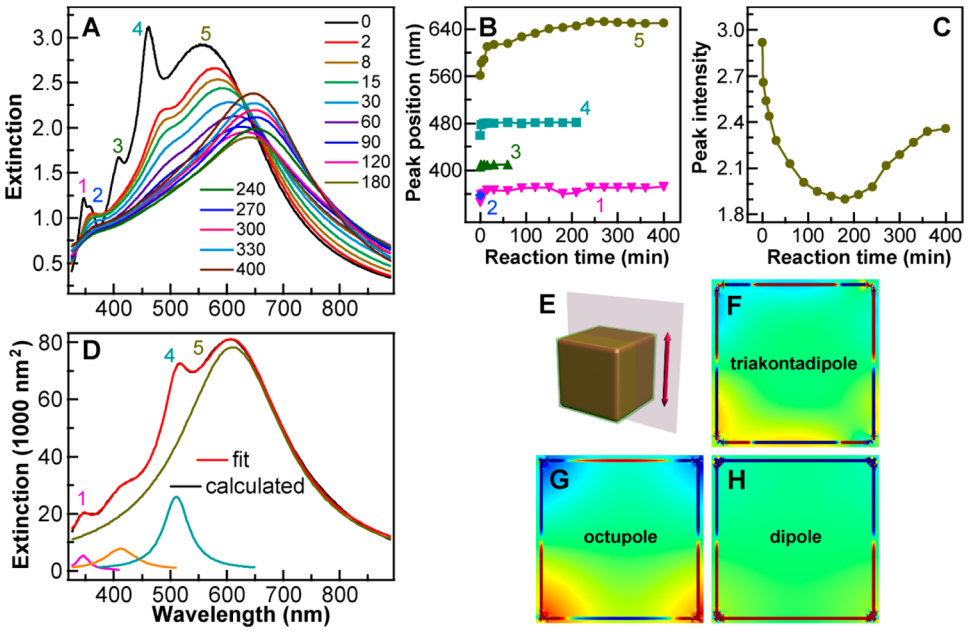

Figure 2. Time-dependent spectral changes over the course of sulfidation of the ensemble Ag nanocube sample with 1 mM Na_2S. (A) Representative extinction spectra of the reaction mixture recorded as a function of the reaction time, the unit of which is minutes. (B) Variations of the peak positions as a function of the reaction time. The peak positions were determined by curve fitting. Some peaks can still be resolved, even though they are submerged under the much stronger peaks and are difficult to see clearly. The peak positions were tracked until the intensities were too weak for fitting. (C) Variation of the extinction intensity of peak 5 as a function of the reaction time. (D) Calculated extinction spectrum of a truncated Ag nanocube with a 3 nm radius of curvature for all the edges. The calculated extinction spectrum is fitted using four Lorentzian peaks, with each peak also plotted. The coefficient of determination for the fitting is 0.9995. (E) Schematic showing the truncated Ag nanocube and the cross section through the center of the nanocube. The double-arrowed line indicates the excitation polarization direction. (F−H) Charge distribution contours (red: positive; blue: negative) on the cross section shown in E for the peaks labeled in D as 1, 4, and 5, respectively. The nature of each plasmon resonance mode is indicated on the charge distribution contour.

large red shifts and reach plateaus by the end of the first stage. The second stage covers from ~10 min to ~400 min. The spectral positions of peaks 1, 3, 4, and 5 change only slightly. Peak 3 disappears after ~60 min, and peak 4 vanishes after ~210 min. Because the other peaks either vanish or are very weak during the sulfidation process, only the extinction intensity of peak 5, which results from a dipolar plasmon resonance mode, is plotted against the reaction time (Figure 2C). Peak 5 exhibits a rapid decrease in extinction intensity within ~30 min after the reaction is started. Its extinction intensity then decreases gradually and reaches a minimum around 180 min, with the intensity at the minimum being 65% of that at the start. After the minimum, the extinction intensity of peak 5 starts to increase slowly. By 400 min after sulfidation is initiated, no further change in the spectral position and intensity of peak 5 is observable. We therefore stopped the extinction spectral monitoring. At this reaction time, the extinction intensity becomes 80% of that at the start, and the peak is located at 651 nm, being red-shifted by 90 nm in comparison to that at the start.

Similar spectral evolutions were also observed when sulfidation was carried out at lower Na_2S concentrations of 0.6 mM (Supporting Information Figure S1) and 0.2 mM (Supporting Information Figure S2). Peak 2 vanishes almost instantly upon sulfidation. Within the first ~10 min after the reaction, the other four peaks show rapid red shifts. After that, their peak wavelengths stay almost unchanged as the sulfidation process proceeds. As the concentration of Na_2S is reduced, the net red shifts of peak 5 from the start to the end of the monitoring process become smaller. The red shifts of peak 5 for sulfidation with 0.6 and 0.2 mM Na_2S are 58 and 34 nm, respectively. At the lower concentrations of Na_2S, the octupolar plasmon modes, peaks 3 and 4, remain longer in the course of the reaction. In addition, the extinction intensity of peak 5 drops to a minimum within 2 min of the reaction for both lower concentrations of Na_2S. The intensity reductions relative to those at the start are small, 5% and 3% for 0.6 and 0.2 mM Na_2S, respectively. This behavior is different from that observed for 1 mM Na_2S. Because the plasmonic spectral properties of metal nanocrystals are determined by the nanocrystal shape, size, and environment, the spectral evolutions observed during the sulfidation process with different concentrations of Na_2S suggest that the sulfidation behavior at the early stage is similar under different concentrations of Na_2S and that the sulfidation behavior at the late stage varies with the concentrations of Na_2S. We also performed the sulfidation experiments with the concentration of Na_2S at 1.5 mM or above. At the higher concentrations of Na_2S, quick aggregation of the Ag

nanocubes was always observed, which prevented us from investigating the time-dependent sulfidation process.

Sulfidation has been reported to initiate at the sharp tips of Ag nanoprisms and nanocubes.[11] We reason that this also occurs with the ensemble Ag nanocube sample in our experiments. At the sharp vertices and edges, the Ag atoms have fewer neighboring atoms and are less capped by the stabilizing molecules.[33,34] They are therefore prone to be attacked by the sulfur-containing species in the solution. From the perspective of surface chemistry, the vertices and edges are the initiation sites on the Ag nanocubes for sulfidation. Since the electric charges associated with peak 2, a triakontadipolar plasmon mode, are mainly located at the surfaces and edges of the Ag nanocube, the nearly instant disappearance of peak 2 upon sulfidation can be ascribed to the preferential truncation of the vertices and edges of the Ag nanocubes. To ascertain this ascription, we performed FDTD simulations on a 93 nm Ag nanocube that was truncated at all the edges, with a truncation radius of 3 nm and the truncated regions replaced with Ag_2S. The simulated extinction spectrum (Figure 2D) is in good agreement with the experimental one (Figure 2A) recorded at 2 min after the reaction. The simulated extinction spectrum exhibits four peaks, at 345, 410, 512, and 610 nm. The peak at 410 nm might be jointly caused by the inaccuracy of the FDTD simulation and the octupolar plasmon mode, as mentioned above. According to their charge distributions (Figure 2E–H), the other three peaks can be taken as corresponding to peaks 1, 4, and 5 of the original perfect Ag nanocube, which are triakontadipolar, octupolar, and dipolar plasmon modes, respectively. Peak 2, a trikontadipolar plasmon mode, is absent. The FDTD simulations therefore confirm that the disappearance of peak 2 right after the start of the reaction is caused by the edge truncation of the Ag nanocubes through sulfidation and, in turn, that sulfidation starts at the vertices and edges of the Ag nanocubes. These results suggest preliminarily that the sulfidation process of Ag nanocubes can be tracked by monitoring the spectral changes of the plasmon resonances.

Structural characterizations were carried out on the sulfidation products that were collected at 2, 30, 150, and 400 min of the reaction with 1 mM Na_2S. SEM imaging (Supporting Information Figure S3) shows that the nanostructures remain cubic with smooth facets during the course of sulfidation. At 400 min, small bumps appear on the surfaces of the nanostructures. They are caused by electron-beam irradiation during SEM imaging. A considerable amount of Ag in each nanostructure is converted into Ag_2S at this reaction time. As reported previously,[35] electron-beam irradiation can decompose Ag_2S to generate Ag nanoparticles on the surfaces of Ag_2S nanostructures. The cubic shape and smooth facets are confirmed by the TEM images (Figure 3A–D) taken on the same products, as seen under SEM. From the TEM images, the average edge lengths of the four intermediate products are found to be slightly enlarged to 95 ± 2, 96 ± 2, 99 ± 4, and 108 ± 5 nm, respectively. Contrast is also observed between the edges and center of the cubic products on the TEM images. It becomes clearer with increasing reaction time, suggesting that Ag is gradually converted into sulfide. Elemental mapping was therefore performed to reveal the composition evolution during sulfidation (Figure 3E–H and Supporting Information Figure S4). S is clearly detected at the edges at 2 min after reaction, confirming again that sulfidation is initiated at the vertices and edges of the Ag nanocubes. With increasing reaction time, the region representing S on the elemental map is enlarged and expanded toward the center. However, no S but Ag is detected from the central region of the cubic nanostructures even at 400 min after reaction. The absence of the S signal in the central region suggests that the Ag nanocubes are not completely converted into sulfides. Incomplete sulfidation is also corroborated by energy-dispersive X-ray (EDX) and X-ray diffraction (XRD) measurements. Although the S molar percentage increases with the reaction time (Figure 3I and Supporting Information Figure S5), it reaches only 18% at 400 min. The XRD patterns of the sulfidation products (Figure 3J and K and Supporting Information Figure S6) can be indexed according to the face-centered-cubic structure of Ag and the monoclinic structure of Ag_2S, indicating the conversion of Ag into Ag_2S during the sulfidation process. The time-dependent XRD patterns also show an increase in the amount of Ag_2S with the reaction time. The S molar percentage in Ag_2S is 33%, much larger than the value at 400 min, confirming again the incomplete sulfidation. The incomplete sulfidation can be ascribed to the slight deficiency in the amount of Na_2S at 1 mM by comparing the estimated amounts of Ag and Na_2S in our experiments according to the stoichiometric reaction given above and the difficulty of S^{2-} diffusion into the center of the nanocube owing to the relatively large size. In addition, the density of Ag_2S (7.2 g cm^{-3}) is smaller than that of Ag (10.505 g cm^{-3}), which explains the increase in the edge length. Complete sulfidation would give a final edge length of 110 nm for the Ag_2S nanocube. This size is slightly larger than the average one measured at 400 min after reaction, which might be due to the measurement deviations and/or that the density of Ag_2S obtained in our experiments is smaller.

Taken together, the structural characterizations show that the sulfidation of the Ag nanocubes starts from the highly reactive vertices and edges and proceeds to form a shell of Ag_2S around each Ag nanocube. The conversion of the vertices and edges into Ag_2S causes the vanishing of peak 2, a triakontadipolar plasmon mode. Continuous sulfidation gradually

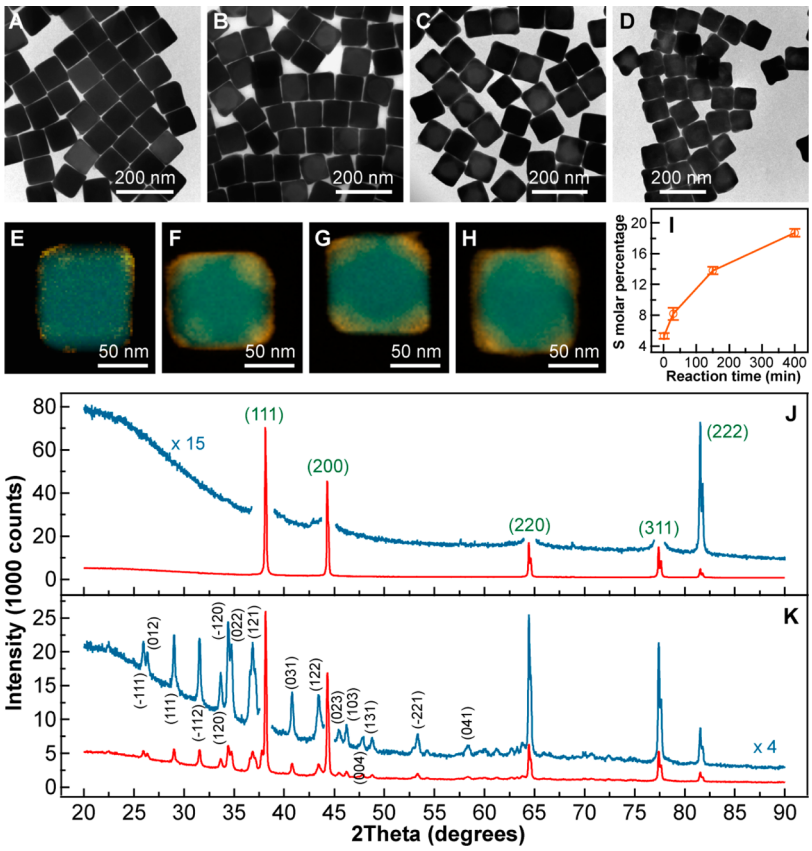

Figure 3. Structural characterizations of the sulfidation products. (A−D) TEM images of the products collected at 2, 30, 150, and 400 min, respectively. (E−H) Merged elemental maps (orange: S; blue: Ag) recorded on the single nanostructures from the products collected at 2, 30, 150, and 400 min, respectively. (I) Increase in the S molar percentage with the reaction time. The content of S was determined by EDX on a SEM system. For each sample, more than eight points were measured. (J, K) XRD patterns of the original Ag nanocube sample and the sulfidation product collected at 400 min, respectively. The patterns are magnified to better reveal the weak diffraction peaks. The diffraction peaks are indexed according to the face-centered-cubic structure of Ag (JCPDS 89-3722, green numbers) and the monoclinic structure of Ag_2S (JCPDS 14-72, black numbers).

reduces the size of the Ag core and increases the thickness of the Ag_2S shell, which is reflected in the extinction spectra as the continuous red shifts and intensity variations of peak 5, a dipolar plasmon mode. The spectral changes of peak 5 are mainly caused by the formation of the Ag_2S shell, which increases in thickness and has a larger refractive index than water. These results indicate that the structural change and the plasmonic evolution are closely correlated with each other. The latter can be employed to help in tracking and elucidating the sulfidation progress.

To eliminate the averaging effect associated with the ensemble measurements as well as highlight the plasmonic sensitivity of the sulfidation products to the structural and environmental changes, we performed the sulfidation reaction at the single-particle level. The measurements employed an optical microscope that was capable of single-particle dark-field scattering spectroscopy[36] together with a microfluidic chip made of poly(dimethylsiloxane) (PDMS) (Figure 4A). The PDMS microchannel was sealed by covering a glass slide that was predeposited with the Ag nanocubes at an appropriate surface number density, with the nanocube-deposited surface facing the microchannel. Before the sealing, the PDMS surface was treated with oxygen plasma to enhance the binding between the PDMS chip and the glass slide. During the sulfidation process, the aqueous Na_2S solution at 1 mM was continuously pumped through the microchannel with a syringe pump. Single-particle scattering spectra were measured as a function of the reaction time.

Figure 4B shows the scattering spectra recorded as a function of the reaction time on a representative Ag nanocube. Only one broad peak is observed on the scattering spectrum before sulfidation (black curve). This peak can be attributed to the dipolar plasmon mode (peak 5) of the nanocube, as discussed above. The observation of only the dipolar plasmon peak is caused by the limit of our optical system in the spectral detection range and the nonradiative nature of the higher-order plasmon modes, which are difficult to detect through far-field scattering signals. The dipolar plasmon peak is located at 608 nm in water before Na_2S is introduced, while the corresponding one for the ensemble sample is at 562 nm. The difference in the peak wavelength is due to the nanocube size

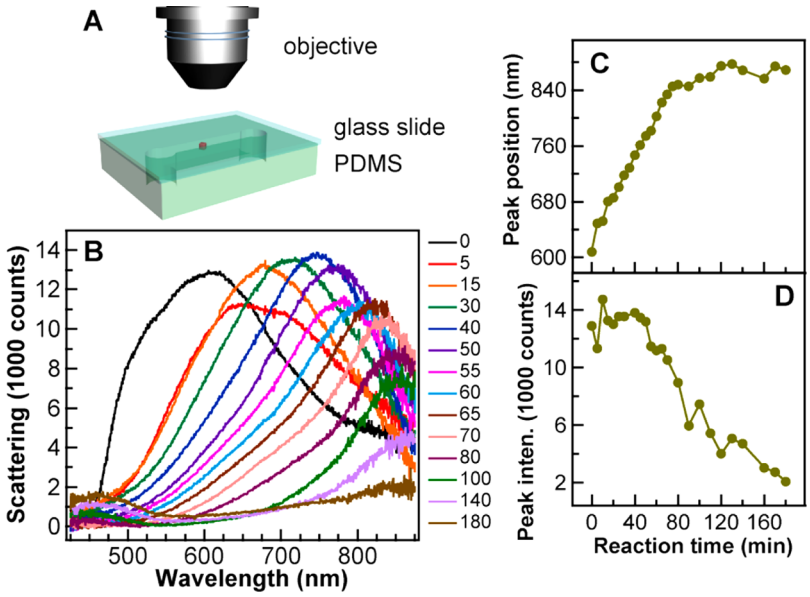

Figure 4. Time-dependent spectral evolution over the course of the sulfidation reaction at the single-particle level with 1 mM Na_2S. (A) Schematic of the setup for measuring the single-particle scattering spectra during sulfidation. The aqueous Na_2S solution was pumped into the microchannel with a syringe pump. (B) Representative scattering spectra collected on a single nanostructure as a function of the reaction time. The labeling numbers stand for the periods of the reaction time, with the unit being minutes. (C) Variation of the spectral position of peak 5 as a function of time. (D) Variation of the scattering intensity of peak 5 as a function of time.

distribution and the higher refractive index of the glass substrate. During sulfidation, the scattering peak red-shifts and gets weaker. The peak position and intensity are extracted and plotted in Figure 4C and D. Similar to the evolution of peak 5 during the ensemble sulfidation process, the variation of the dipolar plasmon peak during the single-particle sulfidation reaction also exhibits two stages. The peak red-shifts rapidly from 608 nm to ~850 nm at the first stage from 0 min to ~80 min. It reaches a plateau and then red-shifts slightly to ~870 nm at the second stage from ~80 min to ~180 min. The overall red shift (~260 nm) observed in the single-particle sulfidation process is much larger than that (~90 nm) in the ensemble sulfidation process. The peak scattering intensity undergoes a gradual reduction throughout the sulfidation process, with an overall decrease of ~85%. This is different from the intensity variation observed in the ensemble sulfidation experiment, where the extinction intensity of peak 5 first decreases, reaches a minimum, and then increases, with the overall intensity reduction being 20%. Moreover, a new broad peak is detected in the spectral region below 500 nm at the later stage of sulfidation, while it is not observed during the ensemble sulfidation process. The wavelength of this new peak cannot be determined exactly because of the limit in the spectral detection range.

FDTD simulations were therefore performed to unravel the reasons for the different spectral evolutions observed during the ensemble and single-particle sulfidation experiments. Two major structural changes are seen experimentally from the ensemble sulfidation products. One is that the chemical composition is changed from Ag to Ag_2S, leading to the concomitant decrease in the Ag core size, while the overall shape of the hybrid particle remains cubic. The other is the overall increase in the edge length of the cubic hybrid particle. The reduction in the Ag core during sulfidation is simulated by first rounding the sharp vertices and edges, with the rounding radius increasing at 6 nm per step (Supporting Information Figure S7). After eight steps of rounding, a Ag nanosphere with its diameter equal to the edge length of the starting Ag nanocube is obtained. After that, the Ag nanosphere is reduced in diameter at 12 nm per step until the Ag core is completely consumed. Throughout the sulfidation process, the volume that is released from rounding and size reduction is filled with Ag_2S, and the overall shape is maintained to be cubic. For comparison, simulations were also performed by retaining the cubic shape of the Ag core throughout the sulfidation process, with the edge length being shrunk at 6 nm per step until the Ag core is consumed (Supporting Information Figure S8A). In both cases, the edge length of the entire cubic particle is fixed at 93 nm, with no change over the course of sulfidation. Fixing the edge length allows for identifying the role played individually by the complex simultaneous structural changes on the plasmon resonances of the sulfidation products. The dielectric functions in the simulations were formulated using Johnson and Christy data for Ag and the data from a previous report[37] for Ag_2S.

The simulated extinction spectra and spectral evolutions of the five plasmon resonance peaks during the

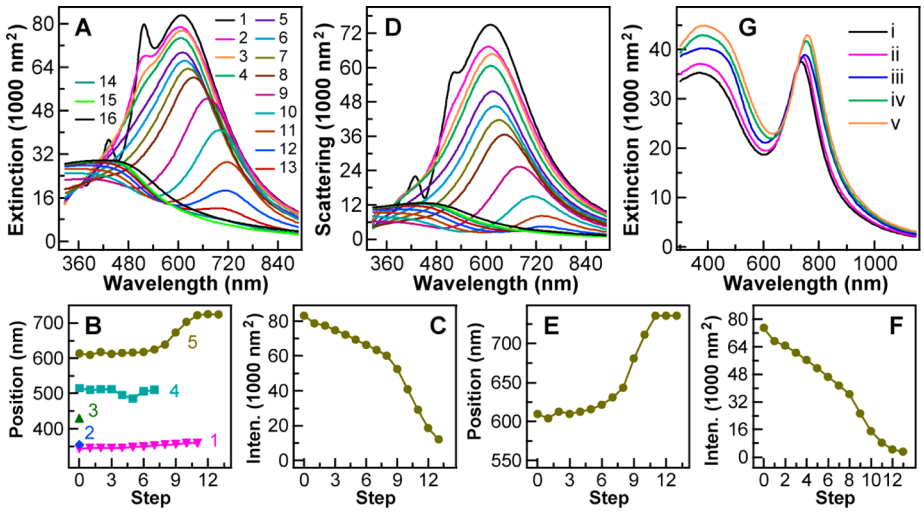

Figure 5. FDTD-simulated spectral evolutions during sulfidation. (A) Simulated extinction spectra at different sulfidation steps. (B) Peak position variations of the five plasmon modes extracted from A as a function of the sulfidation step. (C) Intensity variation of peak 5 extracted from A as a function of the sulfidation step. (D) Corresponding scattering spectra. (E) Position variation of peak 5 obtained from D. (F) Intensity variation of peak 5 obtained from D. (G) Simulated extinction spectra obtained by fixing the size of the Ag core size while increasing the thickness of the Ag_2S shell. The diameter of the spherical Ag core is fixed at 60 nm. The edge lengths of the entire cubic particle are (i) 100 nm, (ii) 102 nm, (iii) 106 nm, (iv) 108 nm, and (v) 110 nm, respectively.

transformation of the Ag nanocube into a nanosphere and subsequent consumption of the Ag core are presented in Figure 5A and B, respectively. Peaks 2 and 3 vanish rapidly. Peaks 1 and 4 stay longer and redshift slightly during sulfidation. In particular, peak 4 disappears when the Ag core becomes a nanosphere. Peak 5 shows a slight red shift of ~5 nm before the Ag core is rounded to become a nanosphere. It thereafter exhibits a more distinct red shift of ~105 nm from ~620 nm to ~725 nm as the Ag core nanosphere is gradually consumed. The extinction intensity of peak 5 first shows a slower decrease and then a rapid decrease, with the transition occurring at the same step as that for the peak position evolution (Figure 5C). The overall intensity reduction is 85%. Meanwhile, a new broad peak shows up around 420 nm and gets stronger after the Ag core becomes a nanosphere. We also obtained the corresponding scattering spectra for the same sulfidation process (Figure 5D), with the evolutions of the position and scattering intensity of peak 5 plotted in Figure 5E and F, respectively. From the scattering spectra, the dipolar plasmon peak redshifts by 125 nm from 610 nm to 735 nm and decreases in intensity by 95% throughout the sulfidation process.

The general evolution trends of the dipolar plasmon peak wavelength and intensity obtained from the simulated scattering spectra are in agreement with those observed from the single-particle scattering measurements. Moreover, at the beginning stage of sulfidation, during which the starting Ag nanocube is gradually truncated into a nanosphere, the general evolution trends of the plasmon peak positions and the extinction intensity of peak 5 agree with those observed from the ensemble sulfidation experiments. There are discrepancies in the spectral evolutions between the experiments and simulations. The discrepancies are believed to arise from the following factors. First, the experimental spectra were taken as a function of the reaction time, while the simulated spectra were obtained as a function of the sulfidation step. It is difficult to correlate the reaction time with the simulation step, especially at the initial sulfidation stage, during which the truncation of the vertices and edges of the Ag nanocube occurs, because the plasmon modes are very sensitive to the truncation degree. Second, there are fluctuations in both the size of the Ag nanocube and the sulfidation process of each nanocube, which affects the comparison between the ensemble sulfidation measurements and the simulations as well as that between the single-particle scattering measurements and the simulations, because the simulations were performed on an averagely sized Ag nanocube. Third, because Ag_2S has a smaller density than Ag, the conversion of Ag into Ag_2S must be accompanied by volume expansion. Since it is difficult to account for these two processes simultaneously, the size of the entire hybrid cubic particles was fixed during our simulations.

On the other hand, two clear discrepancies are seen at the later sulfidation stage between the simulations and ensemble experiments. One is the extinction intensity change of peak 5. It increases in the ensemble sulfidation experiments (Figure 2C), but decreases in the simulations (Figure 5C). The other is the appearance of a broad peak around 420 nm in the simulations (Figure 5A), while this peak is absent in the ensemble experiments (Figure 2A). Both can be ascribed to the incomplete sulfidation of the Ag nanocubes in the

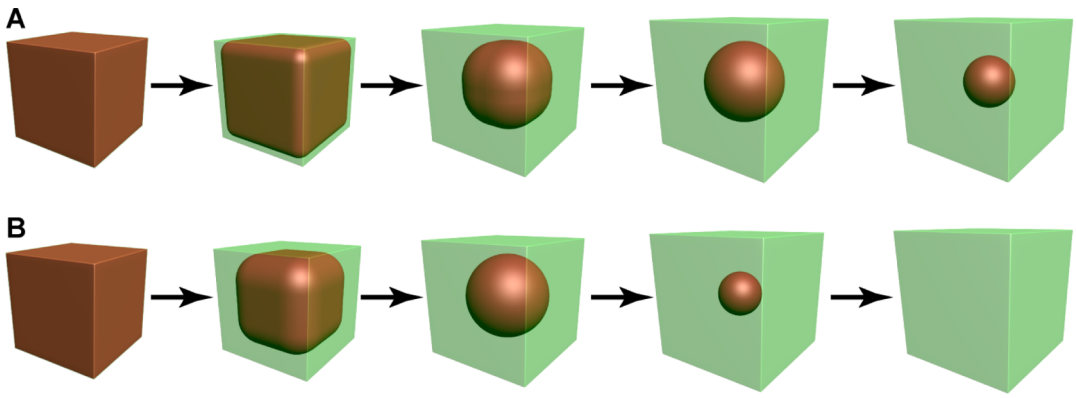

Figure 6. Schematics illustrating the sulfidation processes. (A) Ensemble sulfidation. (B) Single-particle sulfidation. The overall particle size is gradually increased in both cases.

ensemble experiments. The incomplete sulfidation has been verified by the structural characterizations described above. To ascertain the reason for the increase in the extinction intensity of peak 5 at the later ensemble sulfidation stage, we performed FDTD simulations on a hybrid nanocube composed of a 60 nm Ag sphere and a Ag_2S shell. The edge length of the nanocube was increased step-by-step from 100 nm to 110 nm, while the Ag core diameter was fixed. The simulated extinction spectra (Figure 5G) display a slight red shift and an increase in the peak intensity by 14%. Therefore, the sulfidation-caused enlargement of the hybrid nanocubes can account for the extinction intensity increase at the later ensemble sulfidation stage. The difference in the overall trend of the extinction intensity change of peak 5 between the ensemble and single-particle sulfidation experiments is mainly caused by the different sulfidation degrees and the different reaction rates under the two conditions. The broad peak around 420 nm can be ascribed to the absorption and scattering of the Ag_2S shell, because it is also observable on the simulated scattering spectra (Figure 5D) and its extinction intensity is large than its scattering intensity. The simulated extinction and scattering spectra (Figure 5A and D) show that both the extinction and scattering intensities increase with the relative amount of Ag_2S in the hybrid nanocube. The occurrence of this peak is determined by its intensity relative to that of the dipolar plasmon peak of the Ag core, which in turn depends on the relative amounts between Ag and Ag_2S. From the discussion above and according to the observations that the scattering intensity of peak 5 continuously decreases and that a broad scattering peak appears around 420 nm at the later stage in the single-particle measurements, we can reason that the Ag nanocube is completely converted into Ag_2S under the single-particle measurement conditions. The complete sulfidation is understandable, because the Na_2S solution was continuously supplied into the microchannel during the single-particle measurements.

The retaining of a cubic shape for the Ag core over the course of sulfidation is unlikely, as revealed by the simulated extinction and scattering spectra and the extracted position and intensity changes (Supporting Information Figure S8B–G). Although the general trends are qualitatively similar to those observed in the single-particle experiments, the spectral shape is very different from the experimental ones. Two distinct differences are noticed. First, the higher-order plasmon modes, in particular, the octupolar one, cannot be discerned at the beginning sulfidation stage on the extinction spectra, which is in contrast to the ensemble sulfidation experiments. Second, both the extinction and scattering spectra display two peaks above 600 nm as sulfidation goes on. This double-peak feature is not observed in the ensemble nor single-particle sulfidation experiments. Clearly, the simulation results obtained on the assumption that the cubic shape of the Ag core is retained are not in agreement with the ensemble or single-particle experiments. The Ag nanocube must undergo shape transformation during the sulfidation process, with it being increasingly truncated over time.

Taken together, the experimental sulfidation, structure characterization, and FDTD simulation results reveal an overall picture for the sulfidation processes of the Ag nanocubes under both the ensemble and single-particle conditions (Figure 6). In both situations, sulfidation starts from the sharp vertices and edges and progresses toward the center, with a Ag_2S shell formed around the Ag core. The continuous truncation of the Ag nanocube leads to the transformation from a nanocube into a nanosphere. After that, the diameter of the Ag core gets smaller and smaller as Ag is reacted with Na_2S. At this stage, the sulfidation processes start to differ between the ensemble and single-particle experiments. Under the ensemble conditions, the sulfidation process stops at a certain point, forming (Ag core)/(Ag_2S shell) hybrid nanostructures, owing to the insufficient supply of Na_2S (Figure 6A). Under the single-particle conditions, the continuous supply of

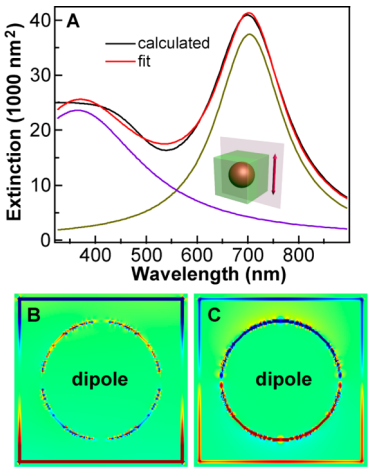

Figure 7. Extinction spectrum and plasmon modes of the (Ag nanosphere core)/(Ag_2S shell) cubic hybrid nanostructure. The diameter of the core is 70 nm, and the edge length of the entire nanostructure is 93 nm. (A) Simulated extinction spectrum of the nanostructure. The spectrum is fitted with two peaks, which are located at 365 and 703 nm, respectively. The coefficient of determination for the fitting is R^2 = 0.9930. The inset is the schematic of the nanostructure and the cross section that passes through the center of the nanostructure showing charge distributions. The double-arrowed line represents the excitation polarization direction. (B) Charge distribution (red: positive, blue: negative) of the 365 nm peak. (C) Charge distribution of the 703 nm peak.

Na_2S leads to the complete sulfidation of the Ag nanocube, producing a Ag_2S nanoparticle (Figure 6B). Under both conditions, throughout the sulfidation processes, the Ag/Ag_2S hybrid nanoparticles maintain the cubic shape with an increase in size due to the smaller density of Ag_2S than that of Ag.

Having elucidated the sulfidation process of the Ag nanocubes, we finally performed FDTD simulations on the (Ag nanosphere core)/(Ag_2S shell) cubic hybrid nanostructure that is formed at the intermediate sulfidation stage to ascertain its plasmon modes. Two peaks are seen on the extinction spectrum (Figure 7A). They are located at 365 and 703 nm, respectively. The charge distributions for the two plasmon resonance peaks are provided in Figure 7B and C. At the 365 nm peak, a small amount of charge is present on the spherical Ag core. The charge distribution shows a mixture of dipolar and higher-order oscillation characteristics. A large amount of charge is present on the outer surface of the Ag_2S shell, with the charge distribution indicating a dipolar mode. The much smaller amount of charge on the Ag core suggests that this peak is dominantly contributed by the charge oscillations in the Ag_2S shell. This observation is in agreement with the reasoning above that the broad peak around 420 nm is mainly contributed by the absorption and scattering of the Ag_2S shell. For comparison, the charge distributions on the Ag core and Ag_2S shell are both dipolar, with the charge intensities being comparable to each other for the 703 nm peak. This result implies that the Ag core maintains the dipolar oscillation in the sulfidation process, even though the dipolar plasmon resonance intensity becomes weaker.

CONCLUSION

In conclusion, we have elucidated the sulfidation process of Ag nanocubes by combining experimental ensemble and single-particle spectral measurements, structural characterizations of the intermediate sulfidation products, and FDTD simulations. Our study shows the high dependence of the strong and rich localized surface plasmon resonance modes of Ag nanocubes on the shape, size, and surrounding environment. The starting Ag nanocubes possess five plasmon modes, with their natures ranging from triakontadipolar to dipolar oscillations. The cubic shape is maintained throughout sulfidation, with an increase in the overall edge length. The quick disappearance of the higher-order plasmon modes with charges mainly localized at the sharp vertices and edges of the nanocube evidences that sulfidation starts at the vertices and edges. The progressive red shifts and intensity evolutions of the other plasmon modes are correlated with the structural changes during the sulfidation process with the assistance of extensive FDTD simulations. The experiments and simulations together show that during sulfidation the Ag nanocube is continuously truncated until it becomes a nanosphere, which is embedded with a Ag_2S shell. After that, the Ag core continuously decreases in diameter. Under the ensemble conditions, sulfidation stops at an intermediate stage, with a Ag nanosphere core remaining. Under the single-particle conditions, sulfidation is complete, with Ag completely converted into Ag_2S. Our study provides an elegant example for employing localized surface plasmon resonances to monitor and guide the chemical transformation of colloidal metal nanocrystals into more complicated hybrid nanostructures with desired plasmonic properties. In particular, the results gained from our study will be useful for preparing Ag/Ag_2S hybrid nanostructures with interesting plasmonic properties from various colloidal Ag nanocrystals.

METHODS

Growth of the Ag Nanocubes. The growth of the Ag nanocube sample followed a reported procedure.[30] Briefly, $CuCl_2$ (60 mM) and PVP (molecular weight: 55 000, 6 mM in terms of the polymer) solutions were first prepared separately by dissolving $CuCl_2$ and PVP in pentanediol completely through ultrasonication and vortexing. A silver precursor solution was made by dissolving $AgNO_3$ (1.2 mmol) in pentanediol (10 mL), followed

by the addition of the preprepared $CuCl_2$ solution (20 μL). Another portion of pentanediol (20 mL) was then added into a 250 mL, three-necked, round-bottom flask and heated to 190 °C in an oil bath. The premade $AgNO_3$ and PVP solutions were alternatively injected into the flask at regular intervals, with the mixture solution in the flask kept at 190 °C. The $AgNO_3$ solution was quickly injected at 0.5 mL every minute, while the PVP solution was added dropwise at 0.25 mL every 30 s. When the addition process was completed, the reaction was quickly stopped by taking the flask out of the oil bath and placing it in an ice-cold water bath. The as-grown Ag nanocube sample was washed three times with an ethanol/water mixture (1:1 by volume) by centrifugation and dispersed in deionized water for further use.

Ensemble Sulfidation. For ensemble sulfidation, an aqueous PVP solution (2.5 mL, 0.002 g mL^{-1}) was first prepared in a glass container. Then 0.3 mL of the as-grown Ag naocube solution was washed according to the procedure mentioned above, dispersed into ethanol (0.1 mL), and then added into the PVP solution. An aqueous Na_2S solution (0.2 mL) at different concentrations was added dropwise to the Ag nanocube solution within 5 s. The final concentration of Na_2S in the reaction solution was controlled at 1, 0.6, and 0.2 mM, respectively. The sulfidation reaction was kept under continuous magnetic stirring and monitored by recording the extinction spectra as a function of the reaction time, until both the peak positions and intensities showed no changes. For each spectral measurement, 1.5 mL of the reaction solution was taken. It was returned back into the reaction container after spectral measurement.

Single-Particle Sulfidation. A simple microfluidic chip was designed to allow for continuous injection of an aqueous Na_2S solution. The microfluidic chip was fabricated with PDMS using standard lithography techniques. The PDMS prepolymer, component A (6.0 g, GE, RTV615), was first mixed thoroughly with the cross-linker, component B (0.6 g). The mixture was then cast on a mold and subjected to polymerization at 65 °C for 1 h. The resultant PDMS block had a thickness of ~4 mm, with parallel microchannels on one surface. The height and width of the channels were 150 and 100 μm. Two holes of ~0.5 mm diameter were made for introducing into and taking out liquid solutions from a microchannel. The Ag nanocubes were deposited on a clean glass slide by immersing the slide in the washed nanocube solution that was diluted by ~10-fold in comparison to the as-grown nanocube solution for ~30 s and then blowing it dry with nitrogen. After the PDMS surface containing microchannels was treated with oxygen plasma (18 W, Harrick Scientific, PDC-32G) for 50 s, it was bound with the nanocube-deposited glass slide. Deionzied water was first pumped in the microchannel through a plastic tube that was inserted into a hole using a syringe pump. An aqueous Na_2S solution (1 mM) was then supplied into the microchannel with another injector. A gas bubble formed in between the water and Na_2S solution flows was used to determine the starting time of the reaction. The solution flowing through the microchannel was led out with another plastic tube that was inserted in the other hole on the PDMS chip. The flow rate of the solution was controlled at ~0.1 mL min^{-1}. Single-particle dark-field scattering spectra were collected as a function of time over the course of sulfidation.

Characterization. Extinction spectra were measured on a Hitachi U-3501 UV/visible/NIR spectrophotometer with cuvettes of 0.5 cm optical path length. XRD patterns were acquired on a Bruker D8 Advance diffractometer with Cu Kα radiation. Elemental mapping was carried out on an FEI Tecnai F20 microscope equipped with an Oxford EDX analysis system. SEM images were taken on an FEI Quanta 400 FEG microscope equipped with an Oxford EDX analysis system. EDX analysis spectra were recorded on the SEM system. Low-magnification TEM imaging was performed on an FEI CM120 microscope.

Single-particle dark-field scattering spectra were recorded on an upright optical microscope (Olympus BX60) that was integrated with a quartz−tungsten−halogen lamp (100 W), a monochromator (Acton SpectraPro 2300i), and a charge-coupled device camera (Princeton Instruments Pixis 512B). During measurements, the camera was thermoelectrically cooled to −70 °C. A dark-field objective (50×, numerical aperture 0.5) was employed for both illuminating individual nanoparticles with white light and collecting scattered light. The scattered spectra from an individual nanoparticle were corrected by first subtracting the background spectra taken from the adjacent region without any nanoparticles and then dividing it with a precalibrated response curve of the entire optical system.

FDTD Simulations. The simulations were performed using FDTD Solution 7.5, developed by Lumerical Solutions, Inc. In the simulations, an electromagnetic pulse in the wavelength range from 300 to 1000 nm was launched into a box containing the target nanoparticle to simulate a propagating plane wave interacting with the nanoparticle. The nanoparticle and its surrounding medium inside the box were divided into meshes of 0.5 nm in size. The refractive index of the surrounding medium was set to be 1.33, which is the index of water. The dielectric functions in the simulations were formulated using Johnson and Christy data for Ag and the previously reported data for Ag_2S.[37] The charge distributions were calculated from the electric field contours using the FDTD software. The size of the Ag nanocube employed in the simulations was set according to the average size measured from the TEM images. The Ag nanocube before sulfidation was assumed to have sharp vertices and edges. The sulfidation process was modeled in two ways. In the first, the Ag nanocube was truncated gradually until it became a nanosphere, which thereafter decreased step-by-step in diameter. The radius for the truncation of the vertices and edges was increased at 6 nm per step. After the Ag core became a nanosphere, its diameter was reduced at 12 nm per step until the Ag core was completely consumed. In the second, the Ag nanocube was assumed to maintain its cubic shape, with its edge length being shrunk at 6 nm per step until the Ag core was completely reacted. Throughout the sulfidation process, the reacted volume of the Ag nanocube was replaced with Ag_2S. The entire nanostructure was kept as a cube.

Conflict of Interest: The authors declare no competing financial interest.

Acknowledgment. This work was supported by Hong Kong Research Grants Council (GRF, Ref. No. CUHK403211, Project Code 2130277 and CRF, Ref. No. CUHK1/CRF/12G, Project Code 2390064). The FDTD simulations were conducted in the High Performance Cluster Computing Centre, Hong Kong Baptist University, which is supported by Hong Kong RGC and Hong Kong Baptist University.

Supporting Information Available: Ensemble sulfidation extinction spectra at different Na_2S concentrations, SEM images, elemental maps, EDX analysis spectra, and XRD patterns of the sulfidation products at intermediate stages, schematics of the sulfidation process, and FDTD-simulated extinction and scattering spectra. This material is available free of charge *via* the Internet at http://pubs.acs.org.

REFERENCES AND NOTES

1. Ming, T.; Chen, H. J.; Jiang, R. B.; Li, Q.; Wang, J. F. Plasmon-Controlled Fluorescence: Beyond the Intensity Enhancement. *J. Phys. Chem. Lett.* **2012**, *3*, 191–202.
2. Chen, H. J.; Shao, L.; Li, Q.; Wang, J. F. Gold Nanorods and Their Plasmonic Properties. *Chem. Soc. Rev.* **2013**, *42*, 2679–2724.
3. Stewart, M. E.; Anderton, C. R.; Thompson, L. B.; Maria, J.; Gray, S. K.; Rogers, J. A.; Nuzzo, R. G. Nanostructured Plasmonic Sensors. *Chem. Rev.* **2008**, *108*, 494–521.
4. Anker, J. N.; Hall, W. P.; Lyandres, O.; Shah, N. C.; Zhao, J.; Van Duyne, R. P. Biosensing with Plasmonic Nanosensors. *Nat. Mater.* **2008**, *7*, 442–453.
5. Chen, H. J.; Ming, T.; Zhao, L.; Wang, F.; Sun, L.-D.; Wang, J. F.; Yan, C.-H. Plasmon−Molecule Interactions. *Nano Today* **2010**, *5*, 494–505.
6. Charles, D. E.; Aherne, D.; Gara, M.; Ledwith, D. M.; Gun'ko, Y. K.; Kelly, J. M.; Blau, W. J.; Brennan-Fournet, M. E. Versatile Solution Phase Triangular Silver Nanoplates for Highly Sensitive Plasmon Resonance Sensing. *ACS Nano* **2010**, *4*, 55–64.

7. Yanik, A. A.; Cetin, A. E.; Huang, M.; Artar, A.; Mousavi, S. H.; Khanikaev, A.; Connor, J. H.; Shvets, G.; Altug, H. Seeing Protein Monolayers with Naked Eye through Plasmonic Fano Resonances. *Proc. Natl. Acad. Sci. U.S.A.* **2011**, *108*, 11784–11789.
8. Lee, Y. H.; Chen, H. J.; Xu, Q.-H.; Wang, J. F. Refractive Index Sensitivities of Noble Metal Nanocrystals: The Effects of Multipolar Plasmon Resonance and the Metal Type. *J. Phys. Chem. C* **2011**, *115*, 7997–8004.
9. Zhang, Q.; Ge, J. P.; Pham, T.; Goebl, J.; Hu, Y. X.; Lu, Z. D.; Yin, Y. D. Reconstruction of Silver Nanoplates by UV Irradiation: Tailored Optical Properties and Enhanced Stability. *Angew. Chem., Int. Ed.* **2009**, *48*, 3516–3519.
10. Goebl, J.; Zhang, Q.; He, L.; Yin, Y. D. Monitoring the Shape Evolution of Silver Nanoplates: A Marker Study. *Angew. Chem., Int. Ed.* **2012**, *51*, 552–555.
11. Zeng, J.; Tao, J.; Su, D.; Zhu, Y. M.; Qin, D.; Xia, Y. N. Selective Sulfuration at the Corner Sites of a Silver Nanocrystal and Its Use in Stabilization of the Shape. *Nano Lett.* **2011**, *11*, 3010–3015.
12. Yan, L.; Jia, H. M.; He, W. W.; Zhang, Y. G.; Mi, L. W.; Hou, H. W.; Zhu, G. S.; Zheng, Z. Hybrid Solar Cells with Outstanding Short-Circuit Currents Based on a Room Temperature Soft-Chemical Strategy: The Case of P3HT:Ag_2S. *J. Am. Chem. Soc.* **2012**, *134*, 17392–17395.
13. Chang, S.; Li, Q.; Xiao, X. D.; Wong, K. Y.; Chen, T. Enhancement of Low Energy Sunlight Harvesting in Dye-Sensitized Solar Cells Using Plasmonic Gold Nanorods. *Energy Environ. Sci.* **2012**, *5*, 9444–9448.
14. Wu, J.-J.; Chang, R.-C.; Chen, D.-W.; Wu, C.-T. Visible to Near-Infrared Light Harvesting in Ag_2S Nanoparticles/ZnO Nanowire Array Photoanodes. *Nanoscale* **2012**, *4*, 1368–1372.
15. Meng, Z.-D.; Ghosh, T.; Zhu, L.; Choi, J.-G.; Park, C.-Y.; Oh, W.-C. Synthesis of Fullerene Modified with Ag_2S with High Photocatalytic Activity under Visible Light. *J. Mater. Chem.* **2012**, *22*, 16127–16135.
16. Nagasuna, K.; Akita, T.; Fujishima, M.; Tada, H. Photodeposition of Ag_2S Quantum Dots and Application to Photoelectrochemical Cells for Hydrogen Production under Simulated Sunlight. *Langmuir* **2011**, *27*, 7294–7300.
17. Zhang, Y.; Hong, G. S.; Zhang, Y. J.; Chen, G. C.; Li, F.; Dai, H. J.; Wang, Q. B. Ag_2S Quantum Dot: A Bright and Biocompatible Fluorescent Nanoprobe in the Second Near-Infrared Window. *ACS Nano* **2012**, *5*, 3695–3702.
18. Hong, G. S.; Robinson, J. T.; Zhang, Y. J.; Diao, S.; Antaris, A. L.; Wang, Q. B.; Dai, H. J. *In Vivo* Fluorescence Imaging with Ag_2S Quantum Dots in the Second Near-Infrared Region. *Angew. Chem., Int. Ed.* **2012**, *51*, 9818–9821.
19. Jiang, P.; Tian, Z.-Q.; Zhu, C.-N.; Zhang, Z.-L.; Pang, D.-W. Emission-Tunable Near-Infrared Ag_2S Quantum Dots. *Chem. Mater.* **2012**, *24*, 3–5.
20. Wang, C. X.; Wang, Y.; Xu, L.; Zhang, D.; Liu, M. X.; Li, X. W.; Sun, H. C.; Lin, Q.; Yang, B. Facile Aqueous-Phase Synthesis of Biocompatible and Fluorescent Ag_2S Nanoclusters for Bioimaging: Tunable Photoluminescence from Red to Near Infrared. *Small* **2012**, *8*, 3137–3142.
21. Du, Y. P.; Xu, B.; Fu, T.; Cai, M.; Li, F.; Zhang, Y.; Wang, Q. B. Near-Infrared Photoluminescent Ag_2S Quantum Dots from a Single Source Precursor. *J. Am. Chem. Soc.* **2010**, *132*, 1470–1471.
22. Morales-Masis, M.; van der Molen, S. J.; Hasegawa, T.; van Ruitenbeek, J. M. Bulk and Surface Nucleation Processes in Ag_2S Conductance Switches. *Phys. Rev. B* **2011**, *84*, 115310.
23. Hodes, G.; Manassen, J.; Cahen, D. Photoelectrochemical Energy Conversion and Storage Using Polycrystalline Chalcogenide Electrodes. *Nature* **1976**, *261*, 403–404.
24. Liang, C. H.; Terabe, K.; Hasegawa, T.; Negishi, R.; Tamura, T.; Aono, M. Ionic–Electronic Conductor Nanostructures: Template-Confined Growth and Nonlinear Electrical Transport. *Small* **2005**, *1*, 971–975.
25. Xu, Z.; Bando, Y.; Wang, W. L.; Bai, X. D.; Golberg, D. Real-Time *in Situ* HRTEM-Resolved Resistance Switching of Ag_2S Nanoscale Ionic Conductor. *ACS Nano* **2010**, *4*, 2515–2522.
26. Wang, R. Y.; Tangirala, R.; Raoux, S.; Jordan-Sweet, J. L.; Milliron, D. J. Ionic and Electronic Transport in Ag_2S Nanocrystal–GeS_2 Matrix Composites with Size-Controlled Ag_2S Nanocrystals. *Adv. Mater.* **2012**, *24*, 99–103.
27. Yang, W. L.; Zhang, L.; Hu, Y.; Zhong, Y. J.; Wu, H. B.; Lou, X. W. Microwave-Assisted Synthesis of Porous Ag_2S–Ag Hybrid Nanotubes with High Visible-Light Photocatalytic Activity. *Angew. Chem., Int. Ed.* **2012**, *51*, 11501–11504.
28. Liu, B.; Ma, Z. F. Synthesis of Ag_2S–Ag Nanoprisms and Their Use as DNA Hybridization Probes. *Small* **2011**, *7*, 1587–1592.
29. Pang, M. L.; Hu, J. Y.; Zeng, H. C. Synthesis, Morphological Control, and Antibacterial Properties of Hollow/Solid Ag_2S/Ag Heterodimers. *J. Am. Chem. Soc.* **2010**, *132*, 10771–10785.
30. Tao, A.; Sinsermsuksakul, P.; Yang, P. D. Polyhedral Silver Nanocrystals with Distinct Scattering Signatures. *Angew. Chem., Int. Ed.* **2006**, *45*, 4597–4601.
31. Zhang, Q.; Li, W. Y.; Moran, C.; Zeng, J.; Chen, J. Y.; Wen, L.-P.; Xia, Y. N. Seed-Mediated Synthesis of Ag Nanocubes with Controllable Edge Lengths in the Range of 30–200 nm and Comparison of Their Optical Properties. *J. Am. Chem. Soc.* **2010**, *132*, 11372–11378.
32. Jiang, R. B.; Chen, H. J.; Shao, L.; Li, Q.; Wang, J. F. Unraveling the Evolution and Nature of the Plasmons in (Au Core)–(Ag Shell) Nanorods. *Adv. Mater.* **2012**, *24*, OP200–OP207.
33. Nørskov, J. K.; Bligaard, T.; Hvolbæk, B.; Abild-Pedersen, F.; Chorkendorff, I.; Christensen, C. H. The Nature of the Active Site in Heterogeneous Metal Catalysis. *Chem. Soc. Rev.* **2008**, *37*, 2163–2171.
34. Kou, X. S.; Sun, Z. H.; Yang, Z.; Chen, H. J.; Wang, J. F. Curvature-Directed Assembly of Gold Nanocubes, Nanobranches, and Nanospheres. *Langmuir* **2009**, *25*, 1692–1698.
35. Liang, C. H.; Terabe, K.; Hasegawa, T.; Aono, M. Resistance Switching of an Individual Ag_2S/Ag Nanowire Heterostructure. *Nanotechnology* **2007**, *18*, 485202.
36. Shao, L.; Fang, C. H.; Chen, H. J.; Man, Y. C.; Wang, J. F.; Lin, H.-Q. Distinct Plasmonic Manifestation on Gold Nanorods Induced by the Spatial Perturbation of Small Gold Nanospheres. *Nano Lett.* **2012**, *12*, 1424–1430.
37. Bennett, J. M.; Stanford, J. L.; Ashley, E. J. Optical Constants of Silver Sulfide Tarnish Films. *J. Opt. Soc. Am.* **1970**, *60*, 224–232.